INTERNATIONAL JOURNAL FOR NUMERICAL METHODS IN FLUIDS, VOL. 21, 75–90 (1995)

A FINITE ELEMENT SIMULATION OF THE CROSS-EFFECTS OF VISCOELASTICITY AND INERTIA IN AN AGITATED VESSEL

D. ANNE-ARCHARD AND H. C. BOISSON

Institut de Mécanique des Fluides de Toulouse, Avenue du Professeur Camille Soula, F-31400, Toulouse, France

SUMMARY

Numerical simulation by a finite element method is used to examine the problem of the rotating flow of a viscoelastic fluid in a cylindrical vessel agitated with a paddle impeller. The mathematical model consists of a viscoelastic constitutive equation of Oldroyd B type coupled to the hydrodynamic equations expressed in a rotating frame. This system is solved by using an unsteady approach for velocity, pressure and stress fields. For Reynolds numbers in the range 0·1–10, viscoelastic effects are taken into account up to a Deborah number *De* of 1·33 and viscoelasticity and inertia cross-effects are studied. Examining the velocity and stress fields as well as the power consumption, it is found that their evolutions are significantly different for low and moderate inertia. These results confirm the trends of experimental studies and show the specific contribution of elasticity without interference of the pseudoplastic character found in actual fluids.

KEY WORDS: numerical simulation; finite element; viscoelasticity; inertia; rotating flow

1. INTRODUCTION

Viscoelasticity is widely encountered in many industrial production systems and, because of its significant impact on the dynamics, must be taken into account in the design of these processes. High viscoelasticity has consequences upon mixing performances, e.g. power consumption or mixing time, and at present the accurate prediction of the flow pattern producing these effects is still very difficult. An extrapolation of Newtonian or pseudoplastic results will not provide the appropriate solution to this problem. Therefore the aim of the present paper is to use numerical simulation to improve the knowledge of the physical phenomena involved in these complex situations for which the experimental approach does not provide a clear understanding.

Indeed, the practical problems encountered in the mixing of non-Newtonian fluids have been studied experimentally. Most of the experiments deal with pseudoplastic fluids, e.g. the work of Metzner and Otto,[1] but very few are devoted to viscoelastic fluids. Moreover, concerning viscoelastic fluids, the published results seems to be inconsistent. For instance, in laminar flows around Rushton turbines, Rieger and Novak[2] and Oliver *et al.*[3] have deduced that the viscoelastic flow is less dissipative than the corresponding Newtonian flow. In contrast, it was found to be more dissipative by Collias and Prud'homme[4] for the same impeller and highly elastic fluids, by Brito de la Fuente *et al.*[5] for a helical ribbon impeller and by Youcefi *et al.*[6] for a paddle impeller. The great diversity of these results arises from the great diversity of the fluids used and also of the dynamics of the considered flows. Thus it is

CCC 0271–2091/95/010075–16

Received July 1993
Revised December 1994

important to clearly identify and separate effects of pseudoplasticity and viscoelasticity as well as to quantify these parameters for the fluids used in experiments.

The values measured in these experiments are global ones: power consumption, mixing time or circulation time. It is clear that a knowledge of the hydrodynamics in the stirrer is necessary to understand and then model the mixing in viscoelastic fluids.[7] These fluids can modify the Newtonian flow patterns and develop large normal stresses, which in turn deeply affect the mixing performances. In this respect a numerical study may be useful even if some simplifications are required to define a tractable equivalent numerical model.

Upon inspecting the power number versus Reynolds number graphs,[5,6] the threshold for which the viscoelastic behaviour diverges from the Newtonian one is generally found in the range $1 < Re < 5$. Similar observations can be made from other experimental results and thus it seems worthwhile to study the cross-effects of viscoelasticity and inertia in homogeneous and isothermal fluids. Numerical simulation of these cross-effects has already been tackled by Delvaux and Crochet[8] for the flow around a circular cylinder and by Debbaut[9] in a circular abrupt contraction where modifications of the flow pattern for a given fluid (and elasticity) are shown as the Reynolds number increases in the range 1–50; strong modifications are noticed even in a reduced range ($Re = 4$–15). In a planar contraction, Choi *et al.*[10] have shown that the corner vortex growth can increase or decrease with increasing Reynolds number depending on whether the fluid elasticity is weak or strong.

To the authors' knowledge, mixing in viscoelastic fluids has not yet been treated numerically. With regard to the mixing of inelastic non-Newtonian fluids, Hu *et al.*,[11] using a finite element method, have provided a numerical solution for the two-dimensional flow of a Carreau A fluid in a vessel with an anchor impeller. Although they did not compute the power number, they have found modifications of the velocity field as the Reynolds number or the power-law index changes. In contrast, for pseudoplastic fluids, Bertrand and Couderc[12] and Lafon[13] have observed small changes in the velocity field but no modifications of the flow pattern, whereas the power number decreases slightly with the power-law index.

In this work we have conducted a numerical simulation of the isothermal flow of a viscoelastic fluid in an agitated vessel with a paddle impeller. The Reynolds number range is fixed in order to introduce significant effects while remaining in the laminar regime. Both the Reynolds and Deborah numbers are sufficiently low to consider that 3D effects are negligible in such a geometry. Experimental data[6] obtained under analogous conditions seem to confirm these assumptions and can be used for qualitative comparison. Furthermore, a 2D approach is more tractable because of the numerous difficulties encountered in numerical simulation of viscoelastic flows.

In Section 2 we present the flow configuration. The basic equations for the problem and the numerical method are described in Sections 3 and 4 respectively. Our main results are presented in Section 5, which is followed by the conclusions in Section 6.

2. THE FLOW CONFIGURATION

This work is mainly concerned with chemical and biological engineering applications. The basic case studied is the flow in a stirring tank equipped with a paddle impeller.

The geometrical configuration in a plane perpendicular to the axis of the tank is shown in Figure 1.

The radii of the vessel and the impeller are R_0 and R_1 respectively. The flow computation will be performed in a Cartesian frame moving with the impeller, which rotates at an angular velocity ω. The Reynolds number will be defined in terms of the rotation frequency $N = \omega/2\pi$ and the impeller diameter D_1. Polar co-ordinates will be used for representing some results in order to compare them with experimental data.

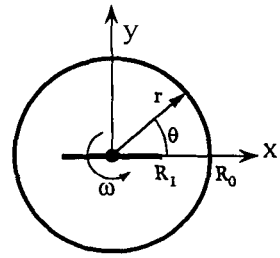

Figure 1. Flow configuration

3. THE GOVERNING EQUATIONS

We solve the incompressible and isothermal flow of a viscoelastic fluid in a domain $\mathscr{D}$. Our problem is then to determine the stress tensor and the velocity and pressure fields. These variables must obey the equations of motion and the incompressibility constraint; for closing the system of equations, we need the constitutive equation for the fluid, i.e. the relation between dynamics (the stress tensor) and kinematics.

We define the rate-of-deformation tensor $\mathbf{D}$ in terms of the velocity field $\mathbf{V}$ as

$$\mathbf{D} = \tfrac{1}{2}(\Delta\mathbf{V} + \Delta\mathbf{V}^{\mathrm{T}}). \tag{1}$$

The stress tensor σ is decomposed as

$$\boldsymbol{\sigma} = -p\mathbf{I} + \boldsymbol{\tau}^*, \tag{2}$$

where p is the pressure and $\boldsymbol{\tau}^*$ is the extra-stress tensor. We use an Oldroyd B law as the constitutive equation for the fluid. This model includes elasticity without any pseudoplastic behaviour. It is characterized by a constant shear viscosity η_0 and a quadratic first normal stress difference:

$$\boldsymbol{\tau}^* + \lambda\overset{\nabla}{\boldsymbol{\tau}}{}^* = 2\eta_0(\mathbf{D} + \lambda_r\overset{\nabla}{\mathbf{D}}). \tag{3}$$

Here λ and λ_r are the relaxation and retardation times respectively and the symbol $^{\nabla}$ holds for the upper-convected derivative, which is an objective time derivation for tensors:

$$\overset{\nabla}{\boldsymbol{\tau}}{}^* = \frac{\partial}{\partial t}\boldsymbol{\tau}^* + (\mathbf{V}\cdot\nabla)\boldsymbol{\tau}^* - \nabla\mathbf{V}\cdot\boldsymbol{\tau}^* - \boldsymbol{\tau}^*\cdot\nabla\mathbf{V}^{\mathrm{T}}. \tag{4}$$

Equation (3) is used in a slightly different way: $\boldsymbol{\tau}^*$ is decomposed into a Newtonian ($\boldsymbol{\tau}_1$) and a viscoelastic ($\boldsymbol{\tau}_2$) contribution as

$$\boldsymbol{\tau}^* = \boldsymbol{\tau}_1 + \boldsymbol{\tau}_2, \tag{5}$$

where

$$\boldsymbol{\tau}_1 = 2\eta_1\mathbf{D}. \tag{6}$$

Since η_1 can be any partial shear viscosity, we choose $\eta_1 = \eta_0\lambda$
$/\lambda$ in order to cancel the coefficient of the time derivative of $\mathbf{D}$ in equation (3). We thus limit the order of derivation for the velocity field $\mathbf{V}$ and the viscoelastic part of the constitutive equation is now

$$\boldsymbol{\tau}_2 + \lambda\overset{\nabla}{\boldsymbol{\tau}}{}_2 = 2\eta_2\mathbf{D}, \tag{7}$$

with $\eta_2 = \eta_0(1 - \lambda_r/\lambda)$.

In order to simplify the notation, $\boldsymbol{\tau}_2$ will be called $\boldsymbol{\tau}$ in the following.

The stress decomposition (5) is introduced into the momentum equation, which is written in a rotating frame with rotational speed ω. This equation is associated with the incompressibility constraint to give the hydrodynamic model

$$\rho\left(\frac{\partial \mathbf{V}}{\partial t} + (\mathbf{V}\cdot\nabla)\mathbf{V} + \mathbf{\Omega}\cdot\mathbf{\Omega}\cdot\mathbf{OM} + 2\mathbf{\Omega}\cdot\mathbf{V}\right) - \nabla\cdot\boldsymbol{\tau} - \eta_1\Delta\mathbf{V} + \nabla p = 0, \tag{8}$$

$$\nabla\cdot\mathbf{V} = 0, \tag{9}$$

where $\mathbf{\Omega}$ is the antisymetric tensor associated with ω and ρ is the fluid density. In our study the moving frame used will be bound to the impeller.

The stress, velocity and pressure fields are the solution of the coupled system formed by equations (5)–(9) together with appropriate boundary conditions.

When studying viscoelastic fluid flows, it is useful to define a measure of the elastic character of the flow by a Deborah number. This number arises naturally in the dimensionless equations as $De = \lambda U_0/L_0$, where L_0/U_0 must be considered as a characteristic time for the flow while λ is a characteristic of the fluid elasticity. In our application the length L_0 and the velocity U_0 used as references are the stirrer radius R_0 and the product ωR_0 respectively, in so far as ω is also the rotational speed of the impeller.

Two other dimensionless groups arise in this application: the Reynolds number $Re = \rho N D_1^2/\eta_0$ and the characteristic time ratio $\beta = \lambda_r/\lambda$.

Taking β equal to zero gives the well-known upper-convected Maxwell model. The time ratio β, i.e. the retardation time λ_r, induces a purely viscous term ($\eta_1 \propto \lambda_r$) in the momentum equations and thus has a stabilizing effect on the numerical results.[14–16] We have adopted the commonly used value of β, namely $\beta = \frac{1}{9}$.[17,18]

4. NUMERICAL METHOD

In a rotating frame bound to the impeller the unsteady problem of the rotation of the impeller becomes a steady problem. Despite the use of this rotating frame for computing, the set of partial differential equations (7)–(9) is treated by a time-marching algorithm, i.e. using a non-steady approach converging to a final steady state. This time approach leads to a decoupled problem with the following algorithm.

Algorithm

For each time step:

Step 1. Solve the constitutive equation (7) for $\boldsymbol{\tau}^{n+1}$, keeping $\mathbf{V}^n$ and p^n fixed.

Step 2. Solve the momentum and mass balance equations (8) and (9) for $\mathbf{V}^{n+1}$ and p^{n+1}, keeping $\boldsymbol{\tau}^{n+1}$ fixed.

Step 3. Check for convergence and start again at the next time step if necessary.

Since we are not interested in the transient flow and in order to obtain lower computational costs, we choose to have no internal iteration at each time step; this results, of course, in an approximate description of the transient flow, which could be reasonably studied, if necessary, by selecting a small enough time step.

For increasing the values of both *Re* and *De*, we use a continuation technique, i.e. starting the new results with the last ones as initial conditions. The first viscoelastic case is initialized with Navier–Stokes results for the velocity and pressure fields and only step 1 is performed at the earlier time stations in order to have a suitable initial stress tensor.

A semi-explicit Euler time scheme is retained for temporal discretization and the equations can be written as follows: for step 1,

$$\frac{3}{De}\boldsymbol{\tau}^{n+1} + \frac{1}{\Delta t}(\boldsymbol{\tau}^{n+1} - \boldsymbol{\tau}^{n}) + (\mathbf{V}^{n}\cdot\nabla)\boldsymbol{\tau}^{n+1} - \nabla\mathbf{V}^{n}\cdot\boldsymbol{\tau}^{n} - \boldsymbol{\tau}^{n}\cdot\nabla\mathbf{V}^{n\mathrm{T}} = \frac{1}{De}(\nabla\mathbf{V}^{n} + \nabla\mathbf{V}^{n\mathrm{T}}); \tag{10}$$

for step 2,

$$\frac{1}{\Delta t}(\mathbf{V}^{n+1} - \mathbf{V}^{n}) + (\mathbf{V}^{n}\cdot\nabla)\mathbf{V}^{n+1} - \frac{\alpha}{Re}\nabla\cdot\boldsymbol{\tau}^{n+1} - \frac{\beta}{2\pi}\frac{1}{Re}\nabla\mathbf{V}^{n+1} + \frac{\alpha}{Re}\nabla p^{n+1} + \boldsymbol{\Omega}\cdot\boldsymbol{\Omega}\cdot\mathbf{OM} + 2\boldsymbol{\Omega}\cdot\mathbf{V}^{n} = 0, \tag{11}$$

$$\nabla\cdot\mathbf{V}^{n+1} = 0. \tag{12}$$

Here $\alpha = (3/2\pi)(1-\beta)$ is a coefficient introduced by the definition of Re and De.

We use a finite element formulation for calculating the fields $\boldsymbol{\tau}$, $\mathbf{V}$ and p over the flow domain $\mathscr{D}$, which is discretized by means of Lagrangian quadrilateral elements. In this way, finite element interpolations are used for the variables τ_{xx}, τ_{xy} and τ_{yy} from the stress tensor, u and v from the velocity field and p. Two different methods are used in this study. In *method 1*, in a classical way for viscoelastic flows, we choose complete biquadratic shape functions for $\boldsymbol{\tau}$ and $\mathbf{V}$ and complete bilinear ones for p. Then a Galerkin method is used to discretize (10)–(12) with integration by parts applied to the highest-order derivatives in the momentum equations. In *method 2*, in order to improve the stability for high elasticity and inertia, we use a method proposed by Marchal and Crochet,[19] based on two ideas: the use of upwinding and bilinear subelements for the stresses. The so-called non-consistent streamline upwind scheme described by Marchal and Crochet is implemented with a subdivision of velocity biquadratic elements into 4×4 parts which are bilinear elements for the stresses.

The previously described algorithm was tested with both methods on Couette flow between concentric cylinders and successfully compared with the analytical solution for this test flow. It was then used on the 4 : 1 abrupt contraction where it provided good results up to $De = 3$ for method 1[20] and up to $De = 20$ for method 2. In the previous study with method 1,[20] effects of inertia were not neglected but remained constant (with $Re = 1$). On the other hand, a preliminary study of the agitated vessel was realized with the Newtonian part of the described algorithm. Calculations were carried out for Reynolds numbers from 0·1 up to 40 and successfully compared with experimental results.[21] Early results for method 1 with viscoelastic fluids in this geometry were carried out in weakly inertial flows ($Re = 0{\cdot}1$) up to $De = 0{\cdot}2$.[22] The tests involving method 2 provide the same results as method 1 in this case.

5. VISCOELASTIC FLUID SIMULATION

5.1. Description of the geometry

The flow domain, defined in the (x, y) plane, is limited by the vessel (radius R_0) and the impeller. The latter is composed of two lateral plates of length $R_1 = \frac{1}{2}R_0$ and thickness $e = 0{\cdot}02R_0$ and an axial cylinder of radius $R_a = 0{\cdot}07R_0$.

The finite element mesh M1 used to discretize the flow domain is shown in Figure 2(a); it consists of 436 velocity elements with a total of roughly 9700 unknowns for method 1 and 25,600 for method 2. The critical zones for the flow are located at the tips of the blades where the mesh is refined.

In order to test the mesh refinement effect, calculations are performed on two different meshes M2 and M3. Mesh M2 differs from mesh M1 only in the blade thickness. The same geometry is maintained between M2 and M3, the latter being refined, especially at the tips of the blades (Figures

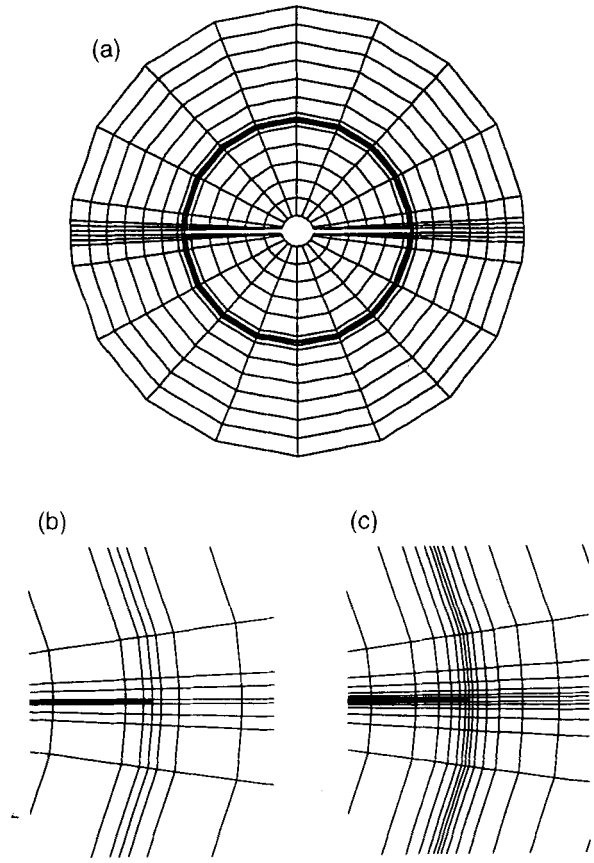

Figure 2. (a) Finite element mesh M1. (b) Details of mesh M2 at tip of blade. (c) Details of mesh M3 at tip of blade

2(b) and 2(c)). M3 consists of 816 elements with about 17,800 or 47,500 unknowns according to the method.

The boundary conditions imposed on the velocity are wall conditions on the impeller and on the outer circular surface. As we choose to work in the rotating frame bound to the impeller, they stand as follows: on the impeller, $V_\theta = V_r = 0$; on the vessel, $V_\theta = -\omega R_0$ and $V_r = 0$. These conditions are expressed in Cartesian components (u, v).

From a mathematical viewpoint there is no complete rule for prescribing boundary conditions for viscoelastic flows in the general case. It has been demonstrated by Renardy[23] that the problem is well posed with Dirichlet conditions for velocity on the boundary $\partial\Gamma$ and no conditions on stresses for the stationary and weakly inertial flow of Maxwell-type fluids, i.e. with a zero retardation time λ_r, if both input and output fluxes are zero everywhere on the boundary. In the present problem the flux conditions at the boundary are realized but the computation is non-stationary and the retardation time λ_r is non-zero. Despite this fact and in the absence of any further theoretical information rigorously adapted to our case, we have considered that Renardy's conditions are relevant. Nevertheless, this choice is reinforced by the results of Guillopé and Saut,[24] showing the well-posedness of the problem when analogous conditions are applied to unsteady flows of Oldroyd-type

Table I. De_{max} for mesh M1

	De_{max}	
	Method 1	Method 2
$Re = 0{\cdot}1$	0·2	1·33
$Re = 10$	0·1	1·33

fluids. However, these results are only demonstrated in the limit of small Deborah number and small parameter a ($a = 1 - \lambda_r/\lambda$).

5.2. Results

We have used both methods of Section 4 to obtain a steady state solution (method 1, centred Galerkin; method 2, non-consistent streamline upwind). The time step varies from 0·1 for the Newtonian case down to 5×10^{-4} for poorly convergent viscoelastic cases. For mesh M1 the value of the maximum Deborah number obtained, De_{max}, depends not only on the Reynolds number but also on the method, as seen in Table I.

The values given in this table are obtained with regular increments of the Deborah number for a given Reynolds number, adapting the time step to the numerical instabilities. They do not provide absolute limits to the method, which could probably be improved with smaller time step or Deborah number increments. Nevertheless, the values obtained with method 1 are limited to low inertial effects or low viscoelastic effects. For this reason, method 2 was chosen in order to obtain large values of Re and De, after having tested the compatibility of both methods in the range of validity of method 1.

Meshes M2 and M3 were used in order to test the effect of mesh refinement. The comparison was done for $Re = 10$ and $De = 1$. The results are identical between the two given meshes for the hydrodynamic field and differ slightly from mesh M1 for which the blade thickness is different. However, discrepancies due to the mesh refinement have been found for the stress field but are only observed near the blade tips: they are attributed to singularities which generate numerical oscillations associated with the size of the mesh.

Looking at the stresses (expressed in polar co-ordinates), we note important local peaks in the vicinity of the tips of the blades as can be seen in Figure 3, representing the normal stress τ_{rr} at different Re for $De = 1{\cdot}33$. A detailed view of the oscillations near the peak value is shown in Figure 4, representing τ_{rr} on the trailing edge for Re increasing from 0·1 to 10.

We can observe more precisely the influence of the Reynolds and Deborah numbers by examining the profiles for τ_{rr}, $\tau_{\theta\theta}$ and $\tau_{r\theta}$ near the leading edge of the plate (Figures 5–7). It is not our objective to discuss here the detailed variations in the stress field, but it is worth noticing that the Deborah number produces large changes in the shape of the peaks for low-inertia flow and that the combined effect of De and Re substantially enhances the amplitude of the peaks. Remembering that $\boldsymbol{\tau}$ is the non-Newtonian part of the stress tensor, this clearly shows the dependence of the viscoelastic part of the extra-stress upon inertia.

Owing to the coupling between stresses and velocity, large modifications in the velocity field are observed in this case. For a better representation, all velocity results obtained in the rotating frame are transformed to be expressed in a fixed frame. The tangential component $\mathbf{V}_\theta$ along the impeller plane is displayed in Figure 8 for four Reynolds number from 0·1 to 10 and four Deborah numbers from 0 to 1·33. Two different behaviours are observed in these curves depending on the Reynolds number. For

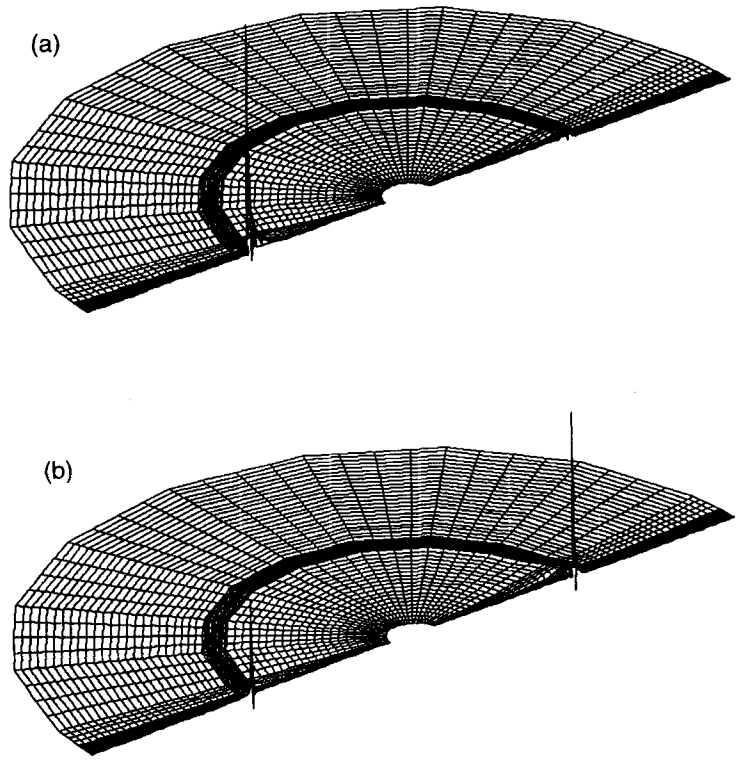

Figure 3. Component τ_{rr} of stress field (leading edge on right): (a) $Re = 0{\cdot}1$, $De = 1{\cdot}33$; (b) $Re = 10$, $De = 1{\cdot}33$

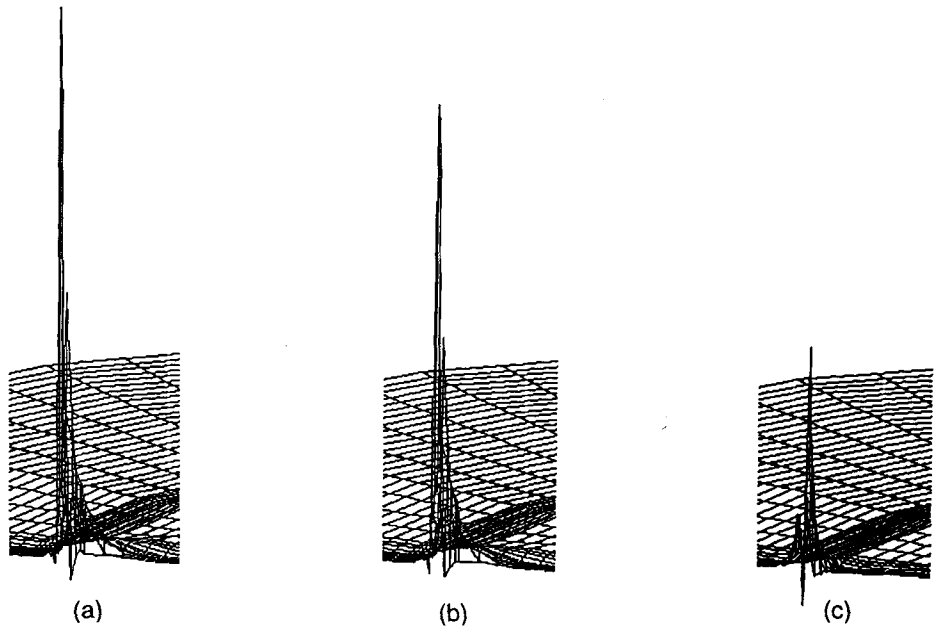

Figure 4. Details of component τ_{rr} of stress field at trailing edge for $De = 1{\cdot}33$: (a) $Re = 0{\cdot}1$; (b) $Re = 1$; (c) $Re = 10$ (identical stress scale for all cases)

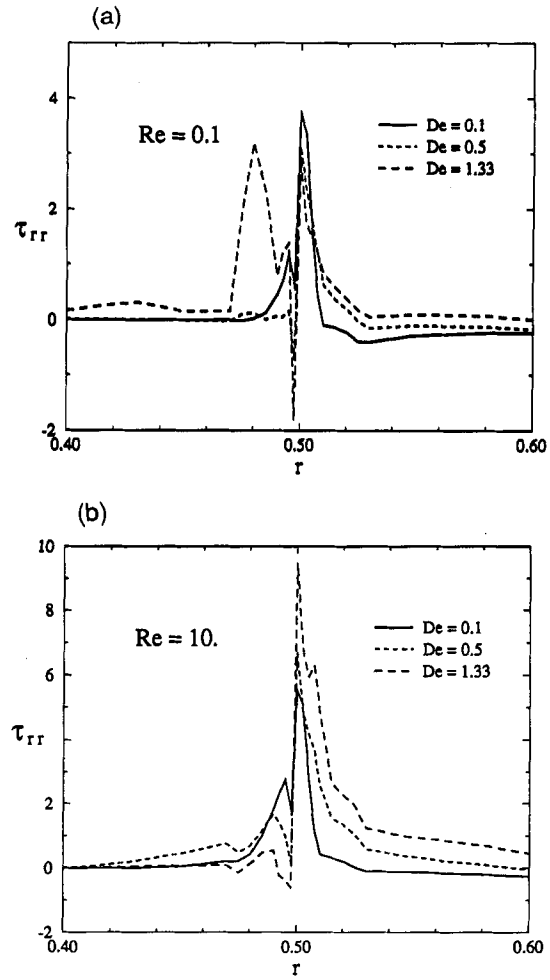

Figure 5. Stress component τ_{rr} on leading edge: (a) $Re = 0{\cdot}1$; (b) $Re = 10$

$Re = 0{\cdot}1$ and 1 the flow velocities in the gap between the blade tip and the wall of the vessel are lower than those in the Newtonian case. The variation with the Deborah number is quite obvious for $De \leq 1$, but the difference is less between the velocity profiles for $De = 1$ and $1{\cdot}33$. The velocity defect is more important at $Re = 1$ than at $Re = 0{\cdot}1$. For $Re = 5$ and 10 and viscoelastic fluids, the velocity profiles in the gap are not monotone as in the Newtonian case but present a minimum near the blade tip and a maximum when moving towards the wall. In our case the Reynolds numbers are sufficiently low and a stable state can be reached. However, it can be inferred that the inflectional profiles obtained are likely to induce shear flow instabilities, which can also limit the range of validity of this steady approach. Another effect of viscoelasticity in the high-Re range is the enhancement of the entrainment of fluid in the gap, which is the opposite of the behaviour for small Reynolds number.

The coupled effect of inertia and viscoelasticity affects the whole domain as can be observed in Figures 9 and 10, showing the streamlines in a fixed frame. The streamfunction ψ is computed from the corresponding velocity field in a postprocessing stage. The low-inertia case is represented in Figures 9(a) and 9(b). A zone of closed streamlines is observed near the wall and in the prolongation of the blade. This zone is nearly symmetrical with respect to the plane of the blade in the Newtonian case

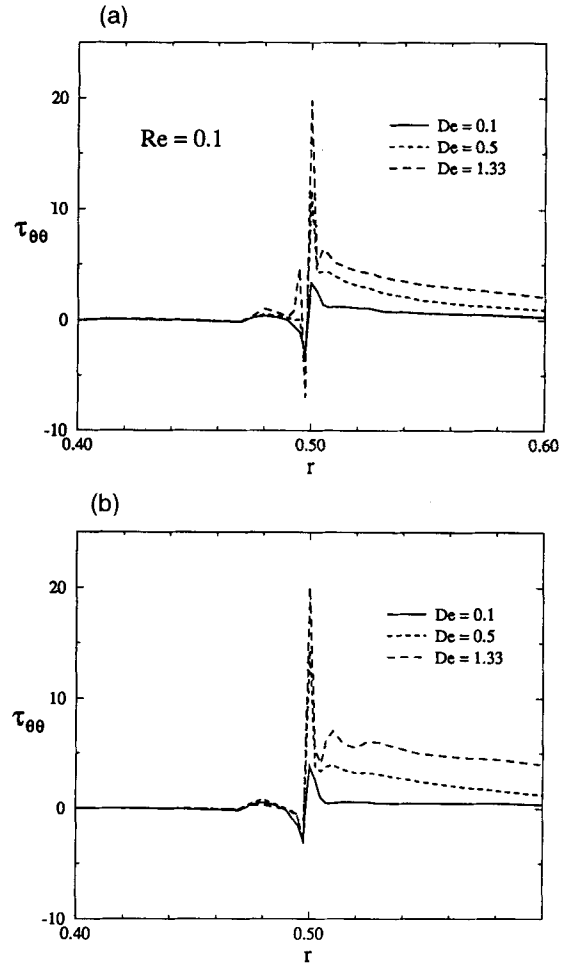

Figure 6. Stress component $\tau_{\theta\theta}$ on leading edge: (a) $Re = 0{\cdot}1$; (b) $Re = 10$

($Re = 0{\cdot}1$, $De = 0$). Viscoelasticity enlarges the surface of this zone and introduces a constant dissymmetry with a quite sharp front on the leading edge side and a tail on the trailing edge side. A decrease in the flow rate is observed with increasing De. A quite different situation is observed with significant inertial effect ($Re = 10$) as shown by Figures 10(a) and 10(b). The closed zones linked to the impeller no longer exist. In the Newtonian case an increase in the entrained flow rate is observed. Viscoelasticity enhances this increase and induces a larger distortion on the streamlines near the impeller as well as a more pronounced dissymmetry with respect to the blade plane. These distortions and dissymmetry are interpreted as supplementary sources of instability introduced by viscoelasticity in inertial flows. An evaluation of the effect of viscoelasticity for different Reynolds numbers in the agitated vessel is given in Table II, representing the maximum value of the streamfunction, $|\psi|_{max}$, and the entrained flow rate which is the value of the streamfunction reached in the vessel, $|\psi|_v$ (since the condition $\psi = 0$ is imposed on the axis of the agitator).

Power consumption is one of the most important industrial parameters, not only from economic considerations but also because it is used as an indicator of the liquid rheology in mixing systems.[7] The power consumption P resulting from the viscous dissipation all over the flow domain $\mathscr{D}$ is defined

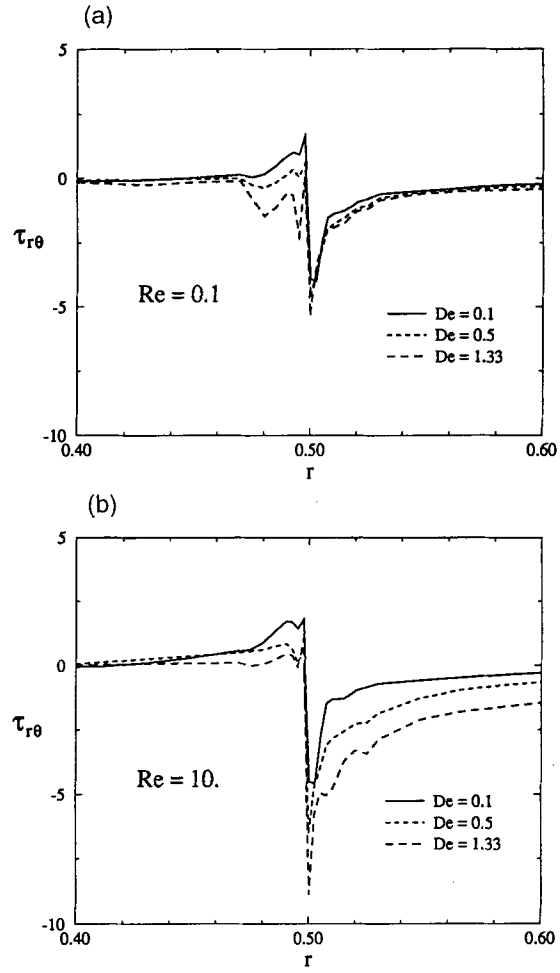

Figure 7. Stress component $\tau_{r\theta}$ on leading edge: (a) $Re = 0{\cdot}1$; (b) $Re = 10$

as

$$P = \int_{\mathscr{D}} \boldsymbol{\sigma} : \mathbf{D} \, dv. \tag{13}$$

The power number, commonly used in mixing processes, is then

$$Np = \frac{P}{\rho N^3 D_1^5}. \tag{14}$$

The computed power numbers are presented in Figure 11, which plots the product $Np{\cdot}Re$ versus the Reynolds number for different values of the Deborah number. Such a dimensionless group takes into account both inertia and viscosity effects. For a given configuration it was found to present small variations for Newtonian fluids as well as for inelastic non-Newtonian fluids, in so far as the Reynolds number is calculated taking pseudoplasticity into consideration.[1,6] Our results show two different regimes. For the lower Reynolds numbers ($Re = 0{\cdot}1$ and 1) the two curves are nearly superposed and

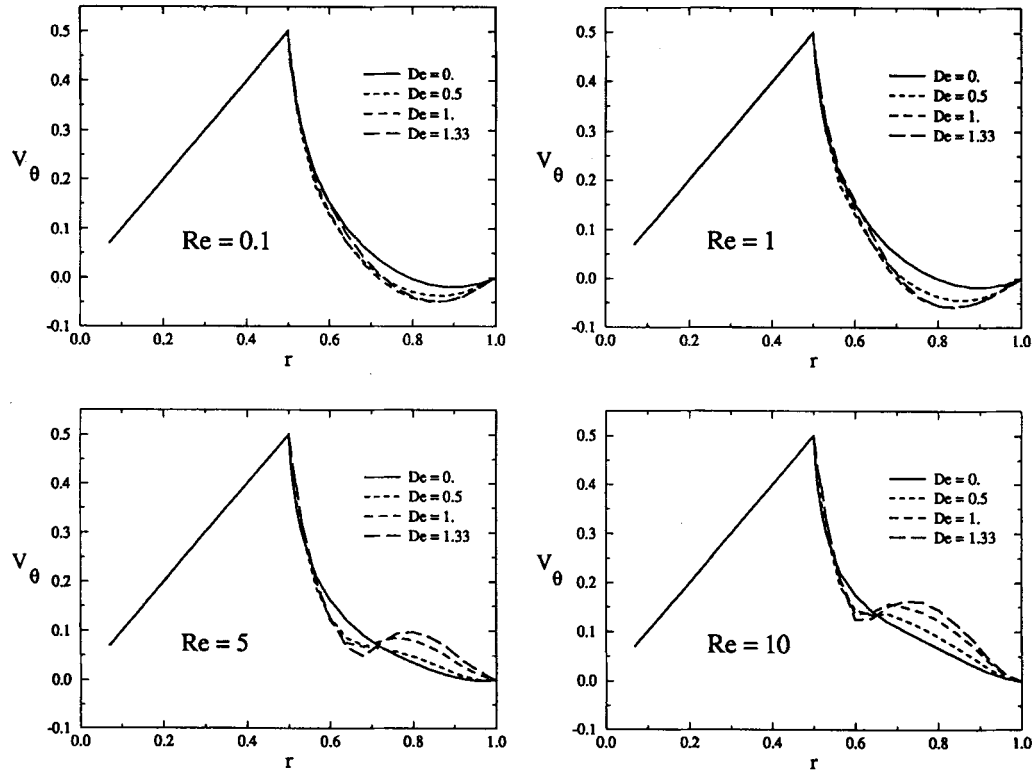

Figure 8. V_θ along impeller and continuation of it

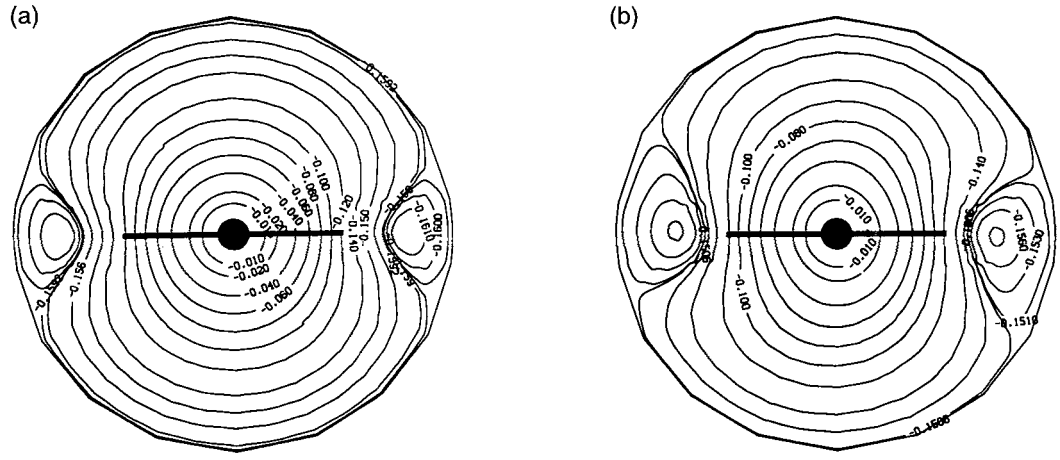

Figure 9. Streamlines for anticlockwise-rotating impeller at $Re = 0{\cdot}1$ (fixed frame): (a) $De = 0$; (b) $De = 1{\cdot}33$

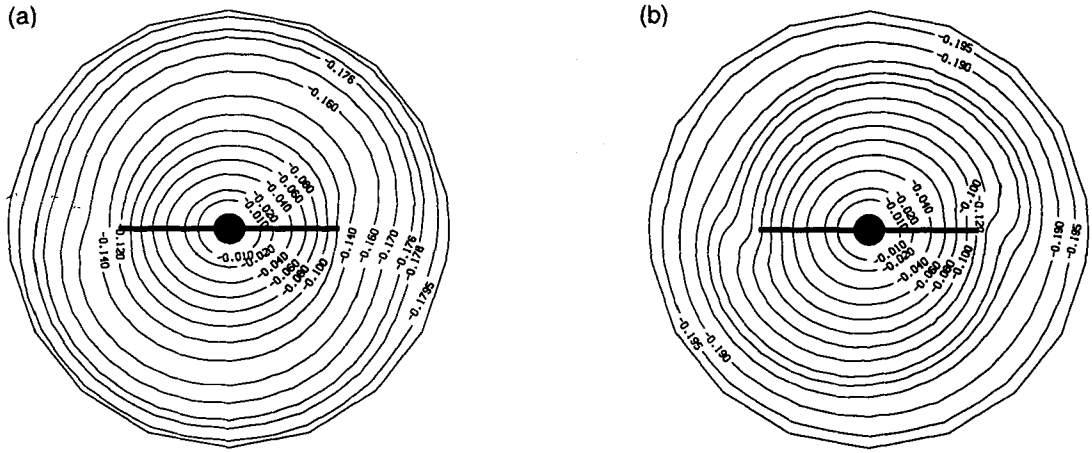

Figure 10. Streamlines for anticlockwise-rotating impeller at $Re = 10$ (fixed frame): (a) $De = 0$; (b) $De = 1{\cdot}33$

both exhibit small variations with respect to the Newtonian case; a small decrease to a minimum for De between 0·5 and 1 is observed. The variation is less than 10% and of the same order as that for Newtonian fluids in the complete Re range studied ($0{\cdot}1 < Re < 10$). In contrast, for the higher Reynolds numbers it is possible to distinguish between two regions in the curves: for small values of De ($De < 0{\cdot}5$) there are no significant modifications of the $Np{\cdot}Re$ dimensionless group, but for larger values of De a substantial increase in this group is observed. For the highest calculated value ($De = 1{\cdot}33$) the power number is increased to nearly 150% of its value for the Newtonian case.

Some results in the literature concerning experimental approaches confirm the previously observed results. Brito de la Fuente *et al.*,[5] Youcefi *et al.*[6] and Carreau *et al.*[25] have observed the same behaviour in the variation of the power with respect to the Reynolds number for viscoelastic fluids. Below a threshold value in the range $0{\cdot}1 < Re^* < 5$ the power number for viscoelastic fluids follows nearly the same law as for inelastic fluids, but beyond this value a substantial departure is observed. In our numerical simulation with an Oldroyd fluid this effect can be unequivocally attributed to the elastic component of the fluid and reveals the importance of the coupled effect of viscoelasticity and inertia.

When studying cross-effects of viscoelasticity and inertia, Debbaut[9] and Choi *et al.*[10] used an elasticity number E. The interest of such a parameter lies in the fact that it is characteristic of the fluid and the geometry regardless of the flow rate and the regime. This number is defined by $E = De/Re$, i.e.

$$E = 2\pi \frac{\lambda \eta_0}{\rho D_1^2}. \tag{15}$$

Another important dimensionless number has been discussed by Joseph *et al.*[26] It represents the importance of propagating effects in a viscoelastic fluid and is also related to the presence of

Table II. Values of $|\psi|_{max}$ and $|\psi|_v$ in the vessel

	$Re = 0{\cdot}1$		$Re = 1$		$Re = 5$		$Re = 10$	
	$\lvert\psi\rvert_{max}$	$\lvert\psi\rvert_v$	$\lvert\psi\rvert_{max}$	$\lvert\psi\rvert_v$	$\lvert\psi\rvert_{max}$	$\lvert\psi\rvert_v$	$\lvert\psi\rvert_{max}$	$\lvert\psi\rvert_v$
$De = 0$	0·1620	0·1593	0·1625	0·1600	0·1703	0·1700	0·1798	0·1797
$De = 1{\cdot}33$	0·1595	0·1507	0·1622	0·1495	0·1791	0·1791	0·1960	0·1960

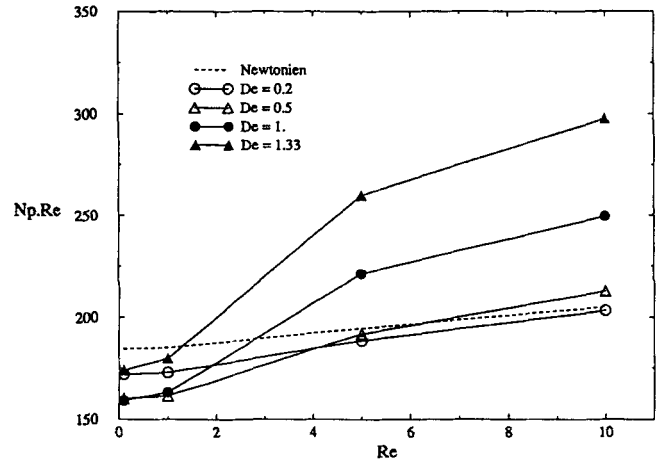

Figure 11. Power number versus Reynolds number: influence of viscoelasticity

hyperbolicity in the equation of motion. This number is the elastic Mach number, defined from the celerity of the elastic waves, $c_0 = \sqrt{(\eta_0/\lambda\rho)}$, so that $M = U_0/c_0$, i.e.

$$M = \sqrt{(2\pi)}\sqrt{(Re \cdot De)}. \tag{16}$$

The previous results can be interpreted with respect to the couple (E, M) rather than (De, Re). In the range covered by this study, the values of E and M are more marked by the Reynolds number values than by the Deborah number. Thus the second regime characterized by high Re and De corresponds to both high Mach numbers and low elasticity numbers. However, completely different flow configurations can be found for comparable values of E, e.g. for the couples (De, Re) = (0·1, 1) and (De, Re) = (1, 10). In contrast, the elastic Mach number provides a better indicator of the regime change. These considerations reinforce the previous observations and show that the differences in the flow patterns for a given fluid and geometry, characterized by the value of E, are closely dependent on the coupled effects of inertia and viscoelasticity, characterized by the value of M.

6. CONCLUSIONS

The rotating flow of a viscoelastic fluid in a cylindrical vessel agitated with a paddle impeller has been studied numerically using a finite element approach. A time-marching algorithm has been chosen to solve the coupled system of fluid constitutive equation and hydrodynamic equations. The latter are expressed in a frame moving with the agitator.

The classical Oldroyd B law is adopted for this simulation, i.e. a viscoelastic but not pseudoplastic fluid. Thus in these simulations the effective viscosity of the flow is constant and the Reynolds number Re directly represents inertia forces. The non-Newtonian contribution is contained in the elastic part which is controlled by the Deborah number De.

The paper deals mainly with the cross-effects of elasticity and inertia for a given level of viscosity upon increasing both De and Re. It is shown that for sufficiently high values of the couple Reynolds number–Deborah number, corresponding to high values of the elastic Mach number, the coupled effect is much higher than each separated effect. This is evident in the evolution of the power number with

respect to the Reynolds number. Obviously the dissipated energy is greater than if only the Reynolds number or the Deborah number was increased separately. The results concerning the power number depart from the classical relationship for Newtonian inelastic flows. The difference noted within the combined inertia–elasticity effect leads to the conclusion that a strong modification of the flow structure has occurred. It appears that the modification in the dissipated energy level, which is closely linked to the flow pattern and the stress field, is due to the presence of viscoelasticity but emerges only through the coupling with inertia.

The method that has been implemented for this study uses a general-purpose algorithm which is not sufficiently sophisticated to overcome all the difficulties of viscoelastic flows. Some specific improvements have been implemented, namely the streamline upwind method and the bilinear subelements for stresses, but progress is still required both in the numerical method and in the constitutive law used for modelling the fluid behaviour.

Nevertheless, this approach can be considered as a first step for this type of problem. It has the merit of enhancing the main characteristics of the inertia–elasticity cross-effect and provides an explanation of experimental observations related to global measures of power consumption.

ACKNOWLEDGEMENTS

The authors wish to thank Professors H. Ha Minh and R. Gaudu for their advice and J.-P. Bombaud for his technical assistance. They are also grateful to 'Centre de Compétence en Calcul Numérique Intensif' CNUSC-IBM for granting them computing time and technical support for vectorization.

REFERENCES

1. A. B. Metzner and R. E. Otto, 'Agitation of non-Newtonian fluids', *AIChE J.*, **3**, 3–10 (1957).
2. F. Rieger and V. Novak, 'Power consumption for agitating viscoelastic liquids in the viscous regime', *Trans. Inst. Chem. Eng.*, **52**, 285–286 (1974).
3. D. R. Oliver, A. W. Nienow, R. J. Mitson and K. Terry, 'Power consumption in the mixing of Boger fluids', *Chem. Eng. Res. Design*, **62**, 123–127 (1984).
4. D. J. Collias and R. K. Prud'homme, 'The effect of fluid elasticity on power consumption and mixing times in stirred tanks', *Chem. Eng. Sci.*, **40**, 1495–1505 (1985).
5. E. Brito de la Fuente, J. C. Leuliet, L. Choplin and P. A. Tanguy, 'On the role of elasticity on mixing with a helical ribbon impeller', *Trans. Inst. Chem. Eng. A*, **69**, 324–331 (1991).
6. A. Youcefi, R. Gaudu, J. Bertrand, D. Anne-Archard and M. Sengelin, 'Mechanical agitation of viscoelastic fluids by a two-bladed stirrer', *The 1992 IChemE Research Event*, Manchester, January 1992, pp. 377–379.
7. J. J. Ulbrecht and P. J. Carreau, 'Mixing of viscous non-Newtonian liquids', in J. J. Ulbrecht and G. K. Patterson (eds), *Mixing of Liquids by Mechanical Agitation*, Gordon and Breach, New York, 1985, Chap. 4.
8. V. Delvaux and M. J. Crochet, 'Numerical prediction of anomalous transport properties in viscoelastic flow', *J. Non-Newtonian Fluid Mech.*, **37**, 297–315 (1990).
9. B. Debbaut, 'On the inertial and extensional effects on the corner and lip vortices in a circular 4 : 1 abrupt contraction', *J. Non-Newtonian Fluid Mech.*, **37**, 281–296 (1990).
10. H. C. Choi, J. H. Song and J. Y. Yoo, 'Numerical simulation of the planar contraction flow of a Giesekus fluid', *J. Non-Newtonian Fluid Mech.*, **29**, 347–379 (1988).
11. H. Hu, J. Wu and X. Fan, 'The numerical simulation of the flow of the Carreau fluid in an agitated vessel with anchor impeller', *Proc. China–Japan Int. Conf. on Rheology*, Beijing, September 1992.
12. J. Bertrand and J. P. Couderc, 'Agitation de fluides pseudo-plastiques par un agitateur bipale', *Can. J. Chem. Eng.*, **60**, 738–747 (1982).
13. P. Lafon, 'Mélange laminaire de fluides miscibles en cuve agitée: approche numérique', *Thèse de Doctorat*, Institut National Polytechnique de Toulouse, 1989.
14. M. J. Crochet, A. R. Davies and K. Walters, *Numerical Simulation of Non-Newtonian Flow*, Elsevier, Amsterdam, 1984.
15. F. Dupret, J. M. Marchal and M. J. Crochet, 'On the consequences of discretization errors in the numerical calculation of viscoelastic flow', *J. Non-Newtonian Fluid Mech.*, **18**, 173–186 (1985).
16. R. Keunings, 'On the high Weissenberg number problem', *J. Non-Newtonian Fluid Mech.*, **20**, 209–226 (1986).
17. R. B. Bird, R. C. Armstrong and O. Hassager, *Dynamics of Polymeric Liquids*, Vol. 1, Wiley, New York, 1977.
18. P. Saramito, 'Simulation numérique d'écoulements de fluides viscoélastiques par éléments finis incompressibles et une méthode de directions alternées. Applications', *Thèse de Doctorat*, Institut National Polytechnique de Grenoble, 1990.

19. J. M. Marchal and M. J. Crochet, 'A new mixed finite element for calculating viscoelastic flow', *J. Non-Newtonian Fluid Mech.*, **26**, 77–114 (1987).
20. D. Anne-Archard, H. C. Boisson and R. Gaudu, 'Simulation numérique de l'écoulement d'un fluide de Bird–Peterlin', *Cahiers Rhéol.*, **8**, 219–236 (1990).
21. A. Youcefi, D. Anne-Archard, H. C. Boisson, M. Sengelin and J. Bertrand, 'Etude numérique et expérimentale de l'écoulement d'un fluide viscoélastique autour d'un agitateur bipale en cuve agitée', in *Collection 'Récents Progrés en Génie des Procédés', Agitation Industrielle*, Vol. 6, No. 19, Lavoisier, Paris, 1992.
22. D. Anne-Archard, H. C. Boisson and H. Ha Minh, 'Finite element simulation of the rotating flow of a viscoelastic fluid', *Proc. XIth Int. Congr. on Rheology*, Brussels, August 1992, Elsevier, Amsterdam, 1992.
23. M. Renardy, 'Existence of slow steady flow of viscoelastic fluids with differential constitutive equations', *Z. Angew. Math. Mech.*, **65**, 449–451 (1985).
24. C. Guillopé and J. C. Saut, 'Résultats d'existence pour des fluides viscoélastiques à loi de comportement de type différentiel', *C.R. Acad. Sci. Paris, Sér. I*, **305**, 489–492 (1987).
25. P. J. Carreau, R. P. Chhabra and J. Cheng, 'Effects of rheological properties on power consumption with helical ribbon agitators', *AIChE J.*, **39**, 1421–1430 (1993).
26. D. D. Joseph, M. Renardy and J. C. Saut, 'Hyperbolicity and change of type in the flow of viscoelastic fluids', *Arch. Rat. Mech. Anal.*, **87**, 213–251 (1985).